European Journal of Soil Science

WILEY

European Journal of Soil Science

RESEARCH ARTICLE

Effects of Physicochemical Properties on Soil Water Vapour Sorption Kinetics

Zizheng Deng | Chong Chen | Xue Song | Jianying Shang | Hu Zhou

Key Laboratory of Arable Land Conservation (North China), Ministry of Agriculture, College of Land Science and Technology, China Agricultural University, Beijing, China

Correspondence: Chong Chen (chenchongsxnd@cau.edu.cn)

Received: 11 February 2025 | **Revised:** 8 August 2025 | **Accepted:** 1 September 2025

Funding: This work was supported by the National Natural Science Foundation of China (42177273) and Chinese Universities Scientific Fund (2024RC015).

Keywords: adsorption rate | cation exchange capacity | condensation | desorption rate | monolayer adsorption | multilayer adsorption | pore volume | specific surface area

ABSTRACT

Soil water vapour sorption kinetics is of great significance to understanding the soil water cycle and soil water vapour movement in arid areas. However, the differences and influencing factors of soil water vapour sorption kinetics in different adsorption processes are still not completely clear. Thus, this study aimed to investigate the soil water vapour adsorption/desorption rates (R_a/R_d) for various water activity (a_w) levels and to identify the key factors affecting these rates. In this study, we determined the change of R_a and R_d with a_w and the R_a and R_d during the monolayer adsorption ($a_w = 0.05–0.02$, R_{a0} and R_{d0}), multilayer adsorption ($a_w = 0.2–0.6$, R_{am} and R_{dm}), and condensation ($a_w = 0.6–0.93$, R_{ac} and R_{dc}) processes for eight mineral soils with different clay contents and mineralogies using a fully-automated AquaLab Vapour Sorption Analyser in dynamic dewpoint isotherm (DDI) mode. Across the entire a_w range, the R_a varied from 2.18×10^{-5} to $1.85\times10^{-4}\,g\,g^{-1}\,min^{-1}$, and the R_d varied from 2.23×10^{-5} to $3.93\times10^{-4}\,g\,g^{-1}\,min^{-1}$. The adsorption rate was in the order of $R_{a0} > R_{am} > R_{ac}$, and the desorption rate was in the order of $R_{dc} > R_{dm} > R_{d0}$. The ratios of adsorption and desorption rates R_{a0}/R_{d0}, R_{am}/R_{dm}, and R_{ac}/R_{dc} are 2.82, 0.97, and 0.48, respectively. The monolayer adsorption rate exceeded its desorption rate, while multilayer adsorption exhibited comparable kinetics to desorption. Adsorption kinetics during capillary condensation exhibited significant retardation compared to desorption dynamics. Cation exchange capacity (CEC) and total specific surface area (SSA) were significant determinants of adsorption–desorption kinetic parameters (R_{a0}, R_{d0}, R_{am}, R_{dm}, and R_{ac}), whereas pore volume (PV) and clay content showed no statistically significant correlation with these kinetic metrics. In contrast, clay content, external SSA, and PV emerged as key factors affecting the R_{ac}, while CEC and total SSA exhibited negligible influence on this parameter.

1 | Introduction

The Global Precipitation Climatology Center (GPCC) reported that the frequency, duration, and intensity of meteorological droughts in West Africa, East Asia, Central America, Amazon River Basin, and Mediterranean region showed an increasing trend to varying degrees from 1951 to 2010 (Spinoni et al. 2014). Moreover, the area affected by meteorological droughts is also expanding (Chiang et al. 2021). Frequent extreme climatic events pose a serious threat to food security and the ecological environment (Mishra and Singh 2010). In an extremely arid environment with limited rainfall and irrigation, non-rainfall water (NRW) comprising dew deposition, fog interception, and vapour adsorption emerges as the dominant mechanism for soil water replenishment (Kidron and Starinsky 2019). Previous studies also reported that vapour adsorption was the main input of NRW resources (e.g., up to 70% of daily evaporation) in arid ecosystems, which generally occurs in the afternoon and evening of

Summary

- Soil water vapour adsorption and desorption kinetics were investigated.
- Soil surface properties play important roles in monolayer and multilayer sorption rates.
- Adsorption rate during condensation was related to soil surface properties.
- Desorption rate during condensation was related to soil nanopores.

a day (Kosmas et al. 1998; Verhoef et al. 2006; Kool et al. 2021). Thus, soil water vapour adsorption is an important process in the water cycle in arid areas (Agam and Berliner 2006; Lopez-Canfin et al. 2022). Understanding this process is essential for improving the utilisation of soil water resources and gaining deeper insight into ecological and environmental changes in arid areas.

Soil water vapour adsorption involves the processes of monolayer adsorption, multilayer adsorption, and condensation (Hatch et al. 2012; Chen et al. 2018). Monolayer adsorption is primarily driven by cation and surface hydration mechanisms (Lu and Khorshidi 2015). Once the monolayer adsorption is finished, the previously adsorbed water molecules can serve as new sites to adsorb other water molecules via hydrogen bonding to form multiple layers (Cheng et al. 2019). With increasing water activity (a_w), the condensation occurs on exposed surfaces, within capillaries, and in the inter-layer of sheet minerals or interspaces of aggregated particles (Li et al. 2016; Sang et al. 2019; Tuller et al. 1999; Yeşilbaş and Boily 2016). Equilibrium adsorption results confirmed that soil water vapour adsorption capacity during the monolayer and multilayer adsorption stages is mainly influenced by cation exchange capacity (CEC) and total specific surface area (SSA). In contrast, the adsorption capacity during the condensation stage is closely related to the external SSA and pore volume (PV) (Song et al. 2022).

Previous studies on soil water vapour sorption have primarily focused on the sorption equilibrium processes, while investigations into sorption kinetics remain relatively limited. The kinetics of water vapour sorption in soils or clay minerals is usually studied by evaluating equilibrium adsorption at discrete a_w intervals (Grismer 1987; Xiong et al. 2023; Sun et al. 2024). However, the limitation of this method is that it can only assess the sorption kinetics within a specific a_w range. Recently, a fully automated and highly sensitive AquaLab Vapour Sorption Analyser (METER Group Inc., Pullman, WA, USA) was developed and can be used to obtain highly detailed adsorption/desorption isotherms operated in Dynamic Dewpoint Isotherm (DDI) mode. Akin and Likos (2020) employed this technique to investigate water vapour sorption kinetics in clay minerals and mineral soils, revealing that the adsorption rate increased with increasing the cation heat of hydration at $a_w < 0.1$, and that at $a_w = 0.25$ showed an extremely significant positive correlation with total SSA. However, their analysis mainly focused on the water vapour adsorption rate for low a_w levels during the adsorption process. Notably, the mechanisms and key influencing factors of soil water vapour sorption vary substantially across different adsorption processes and directions (Lu and Khorshidi 2015; Song et al. 2022), which may significantly impact sorption kinetics. Nonetheless, the differences in soil water vapour sorption kinetics during different adsorption processes and the underlying causes are not completely clear.

In this study, we hypothesise that the adsorption and desorption rates during the monolayer and multilayer adsorption processes are related to soil particle size distribution, SSA, and CEC, whereas the rates during the capillary condensation process are mainly related to the number of soil nanopores. Thus, the objectives of this study were to investigate the soil water vapour adsorption/desorption rates for various a_w levels and to identify the key factors and mechanisms that affect these rates. In this study, the organic matter (OM) was removed from the investigated soils, and its effect on water vapour sorption kinetics was not considered, so we only focused on the water vapour sorption kinetics of mineral soils.

2 | Materials and Methods

2.1 | Sample Collection and Treatments

The eight soils with varying clay contents (6%–47%) and clay mineralogies were used to investigate the soil water vapour adsorption and desorption rates during different adsorption processes. The eight soils used in this study are the same as described in Song et al. (2022). Although this study employed the same set of samples as Song et al. (2022), it focused on sorption kinetics, in contrast to the emphasis on sorption equilibrium in their study. Therefore, the two studies differ substantially in their scientific focus and research objectives. These soils were sampled from the top layer (0–20 cm), subsequently air-dried, crushed, and passed through a 2-mm sieve. The samples were treated with H_2O_2 to remove OM to eliminate the influence of OM on water vapour sorption (Wang et al. 2011). Specifically, approximately 300 mL of 30% (mass fraction) H_2O_2 was introduced to 100 g soil in a beaker, and the mixture was allowed to react thoroughly. Subsequently, the beaker was heated to 80°C to degas the excess H_2O_2. Finally, the treated soil was air-dried, crushed, and passed through a 2-mm sieve.

2.2 | Laboratory Measurements and Analysis

Particle size distribution was determined using the pipette method (Gee and Or 2002). The CEC was determined using the ammonium acetate method at pH 7 (Sumner and Miller 1996). Clay mineral composition was determined with a Rigaku X-ray diffractometer (Smartlab-3kw; Rigaku Corp., Tokyo). The nitrogen adsorption isotherms (77 K) were measured using a Belsorp-max BET Sorptometer (Bel Japan Inc., Tokyo, Japan). Thermogravimetric and X-ray diffraction analyses of heat-treated clay minerals (e.g., montmorillonite) and natural soils revealed that prolonged heating at 150°C did not alter their crystallographic structure (Cases 1997; Araya et al. 2016; Song et al. 2023). Thus, prior to conducting the N_2 adsorption measurement, the sample underwent a degassing process at 150°C for ~12 h to eliminate any interference caused by adsorbed water molecules. Soil specific surface area based on

TABLE 1 | Sampling locations, soil types (FAO soil classification system), and physicochemical properties of the eight investigated soils.

Soil ID	Sampling location	Soil classification	Sand (%) 50–2000 μm	Silt (%) 2–50 μm	Clay (%) < 2 μm	CEC cmol kg^{-1}	SSA_{N2} m^2 g^{-1}	SSA_{H2O} m^2 g^{-1}	Pore volume cm^3 g^{-1}	Clay types
JX	Jiangxi, China (117°2′E, 28°14′N)	Ferric Acrisol	21	32	47	18.4	21	32	0.088	1:1
HN	Henan, China (112°5′E, 32°41′N)	Calcic Vertisols	16	50	34	28.6	19	85	0.038	2:1
JL	Jilin, China (125°31′E, 44°8′N)	Haplic Chernozem	26	47	27	25.4	20	76	0.030	2:1
SD	Shandong, China (116°18′E, 37°27′N)	Haplic Luvisol	26	48	26	16.2	14	40	0.034	2:1
HLJ1	Heilongjiang, China (127°21′E, 47°39′N)	Luvic Phaeozems	27	58	15	28.5	17	64	0.033	2:1
HLJ2	Heilongjiang, China (126°58′E, 45°32′N)	Haplic Chernozem	12	78	10	27.5	12	81	0.028	Mixed
HB	Hebei, China (114°53′E, 40°48′)	Gypsic Kastanozems	67	23	10	12.3	4	26	0.014	2:1
XJ	Xinjiang, China (87°46′E, 43°95′N)	Duric Gypsisols	48	46	6	15.0	6	20	0.018	2:1

nitrogen (SSA_{N2}) was calculated using nitrogen adsorption data using the Brunauer–Emmett–Teller (BET) method (Brunauer et al. 1938), and the PV was determined from the amount of nitrogen adsorbed at the maximum relative gas pressure $P/P0$ of 0.98. The soil water vapour sorption isotherms were determined with a fully automated AquaLab Vapour Sorption Analyzer (METER Group Inc., Pullman, WA, USA). The instrument was configured to operate in the DDI mode across an a_w range of 0.05 to 0.93 with an a_w resolution of 0.02, an air flow rate of 100 mL min^{-1}, and a temperature of 25°C. The DDI mode of the instrument integrates chilled-mirror dewpoint sensing and high-precision microbalance measurements (0.1 mg sensitivity) to dynamically evaluate a_w and water vapour sorption behaviour. The chilled mirror detects condensation temperature to determine a_w (±0.003 accuracy), while the microbalance monitors real-time mass changes, achieving equilibrium when fluctuations drop below the preset threshold. By dynamically adjusting a_w to simulate environmental conditions, the system generates sorption isotherms. Approximately 3.0 g of air-dried samples were used for each measurement. Following isotherm measurements completed, samples were oven-dried to a constant weight at 105°C to determine the soil water content. Water vapour sorption isotherms were measured in duplicates for all soil samples. As the results of the two replicates were highly consistent, only the first measurement was used in subsequent analyses to streamline data interpretation. The specific surface area based on water vapour (SSA_{H2O}) was derived from the water vapour adsorption isotherm using the Guggenheim-Anderson-Boer (GAB) equation (van den Berg and Bruin 1981). Here, SSA_{N2} represents the external SSA, and SSA_{H2O} represents the total SSA of the soil. The physicochemical properties and relative content of the main clay minerals in the eight soils are presented in Table 1 and Table S1.

The time spent at each a_w increment (0.02) was recorded automatically by the Vapour Sorption Analyser, from which the change curves of water content over time were obtained. Based on the water contents at the selected time interval, we calculated the vapour sorption rates (R) at different a_w levels.

$$R = \frac{\Delta\theta}{\Delta t} \tag{1}$$

where $\Delta\theta$ and Δt represent the change in water content (g g^{-1}) and the selected time interval (min), respectively. The following symbols R_a and R_d represent the adsorption and desorption rate, respectively. Figure 1 shows an example of calculating the R of montmorillonite using water vapour sorption measurement.

In soil vapour sorption studies, the a_w thresholds separating monolayer adsorption, multilayer adsorption, and capillary condensation processes are generally set at 0.2 and 0.6, respectively (Akin and Likos 2014; Chen et al. 2018; Chen et al. 2022). Thus, the measured sorption data were divided into three a_w ranges (0.05–0.2, 0.2–0.6, and 0.6–0.93), and the R_a and R_d in the three a_w ranges were calculated. The R_a in these ranges is denoted as R_{a0} (monolayer adsorption), R_{am} (multilayer adsorption), and R_{ac} (capillary condensation), respectively. Similarly, the R_d in the three ranges is denoted as R_{d0}, R_{dm}, and R_{dc}, respectively.

2.3 | Statistical Analysis

To investigate the factors affecting R_a and R_d during three different adsorption processes, the Pearson's correlation analyses between selected soil properties and variables were performed with OriginPro 2022. A significance level of 0.05 and 0.01 was used throughout the study.

3 | Results

Figure 2 presents the changes of R_a and R_d with a_w for the investigated eight soils. Across the entire a_w range, the R_a varied from 2.18×10^{-5} to 1.85×10^{-4} g g^{-1} min^{-1}, and the R_d varied from 2.23×10^{-5} to 3.93×10^{-4} g g^{-1} min^{-1}, indicating that the R_d exhibited a larger variation range relative to R_a. The R_a did not have a consistent change pattern with increasing a_w. For HN, JL, SD, HLJ1, and HLJ2, the R_a first decreased gradually, then changed slightly, and finally decreased gradually with increasing a_w (Figure 2b–f). For JX, HB, and XJ, the R_a showed a small change with a_w (Figure 2a,g,h). For all soils, the R_a showed a decreasing trend with increasing a_w for $a_w > \sim0.8$. As the a_w decreased, the R_d for all soils first increased to a maximum at $a_w = \sim0.85$, and then gradually decreased. In general, R_a was higher than R_d in the low a_w range, the difference between R_a and R_d was small in the medium a_w range, and R_a was lower than R_d in the high a_w range.

Figure 3 compares the R_a and R_d for eight soils during the three sorption processes. During the monolayer adsorption process, the R_{a0} ranged from 5.90×10^{-5} to 1.75×10^{-4} g g^{-1} min^{-1}, while the R_{d0} varied between 2.37×10^{-5} and 5.56×10^{-5} g g^{-1} min^{-1}. The ratio of R_{a0} to R_{d0} was 2.82 ± 0.29 (Figure 3a,b). The R_{a0} was in the order of HN > JL, HLJ2 > HLJ1, SD > JX, HB > XJ. Meanwhile, the R_{d0} was in the order of HN, HLJ2 > JL, HLJ1 > SD > JX, HB > XJ. During the multilayer adsorption process, the R_{am} ranged from 4.37×10^{-5} to 1.47×10^{-4} g g^{-1} min^{-1}, and the R_{dm} varied between 4.64×10^{-5} and 1.29×10^{-4} g g^{-1} min^{-1}. The R_{am}/R_{dm} ratio was 0.97 ± 0.15 (Figure 3c,d). The R_{am} was in the order of HN > JL, HLJ1 > HLJ2 > SD > JX, HB > XJ. Similarly, the R_{dm} was in the order of HN > JL, HLJ2, HLJ1 > SD, JX > HB > XJ. During the capillary condensation process, the R_{ac} ranged from 5.43×10^{-5} to 1.07×10^{-4} g g^{-1} min^{-1}, and the R_{dc} varied between 1.08×10^{-4}

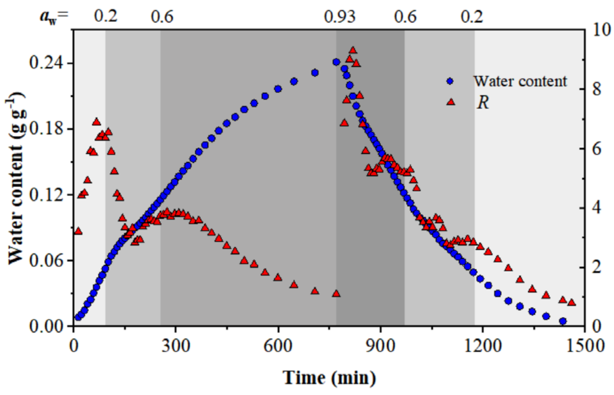

FIGURE 1 | An example of calculating the water sorption rate (R) of montmorillonite using water vapour sorption measurement.

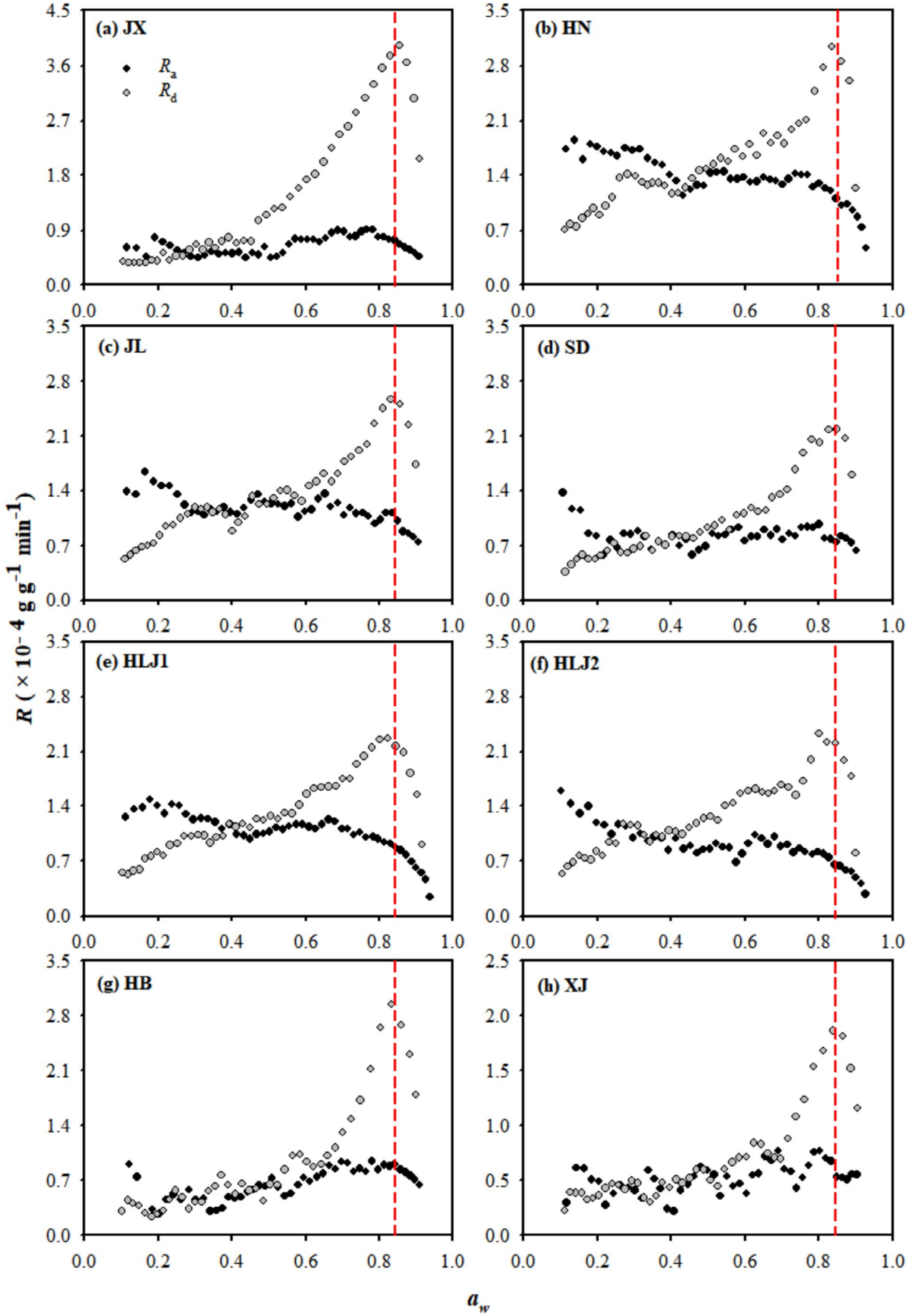

FIGURE 2 | Legend on next page.

FIGURE 2 | The change of adsorption and desorption rates (R_a and R_d) of eight mineral soils with a_w. Soil samples: JX (Jiangxi, a), HN (Henan, b), JL (Jilin, c), SD (Shandong, d), HLJ1 (Heilongjiang, first sample, e), HLJ2 (Heilongjiang, second sample, f), HB (Hebei, g) and XJ (Xinjiang, h) in China. The red line represents the a_w equal to 0.85, and the desorption rate is maximum near this a_w.

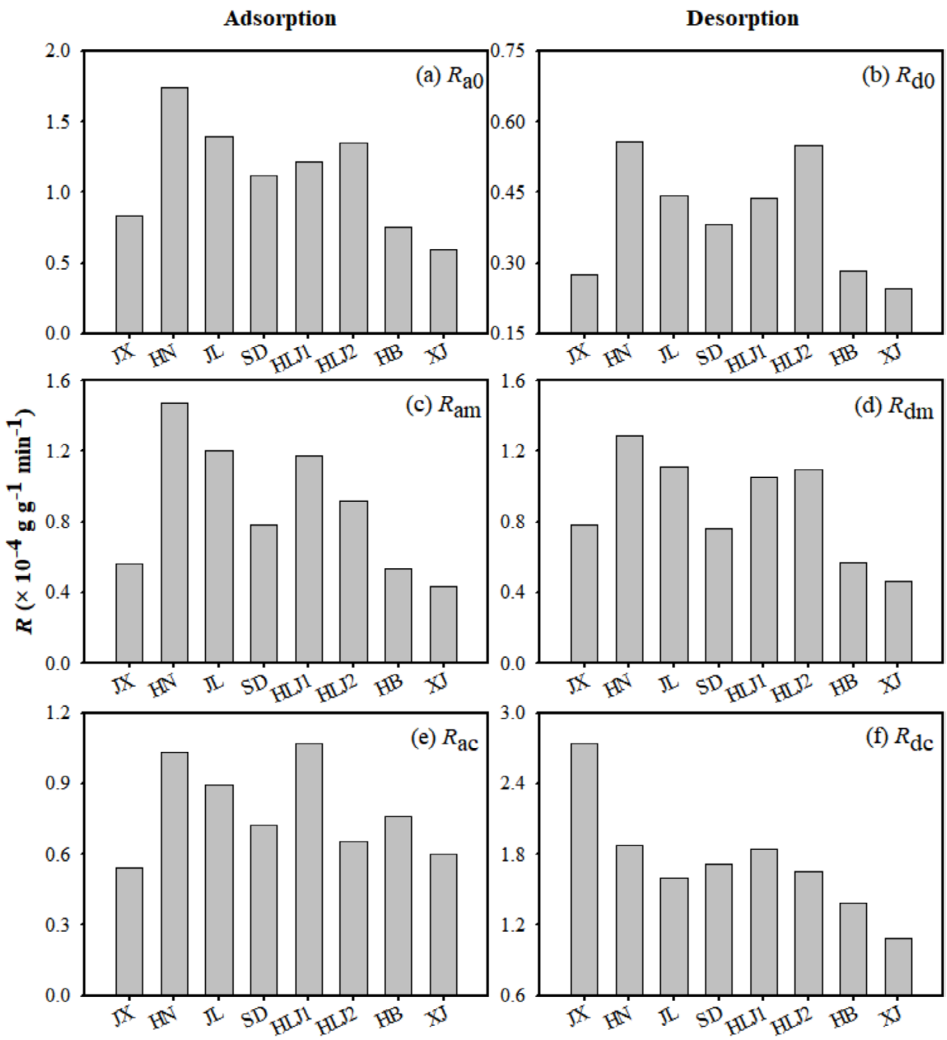

FIGURE 3 | Adsorption/desorption rates of eight mineral soils in different a_w ranges. The R_{a0}/R_{d0} (a, b), R_{am}/R_{dm} (c, d) and R_{ac}/R_{dc} (e, f) are the adsorption/desorption rates during the monolayer adsorption ($0.05 < a_w < 0.2$), multilayer adsorption ($0.2 < a_w < 0.6$), and condensation processes ($0.6 < a_w < 0.93$), respectively.

and 2.75×10^{-4} g g^{-1} min^{-1}. The R_{ac}/R_{dc} ratio was 0.48 ± 0.13 (Figure 3e,f). The R_{ac} was in the order of HN, HLJ1 > JL > HB, SD > HLJ2, XJ > JX, while the R_{dc} was in the order of JX > HN, HLJ1 > SD, HLJ2, JL > HB > XJ.

Correlation analysis revealed that R_{a0}, R_{d0}, R_{am}, and R_{dm} exhibited a highly significant positive correlation with CEC and SSA_{H2O} ($r = 0.85$–0.97; $p < 0.01$) (Figure 4). The R_{ac} showed a higher positive correlation with CEC and SSA_{H2O} than with other soil properties. The R_{dc} showed a significant positive correlation with clay content, SSA_{N2}, and PV ($r = 0.75$–0.96; $p < 0.05$). The results indicated that R_{a0}, R_{d0}, R_{am}, R_{dm}, and R_{ac} were closely related to CEC and SSA_{H2O}, and R_{dc} was closely related to clay content, SSA_{N2}, and PV.

4 | Discussion

During the monolayer adsorption, cation hydration is the dominant mechanism controlling water molecule adsorption on mineral soils (Low 1961; Lu and Khorshidi 2015). The CEC reflects the number of cations adsorbed on the surface of mineral soils and is closely related to SSA_{H2O}. Consequently, monolayer adsorption capacity is significantly positively correlated with CEC and SSA_{H2O} (Khorshidi and Lu 2017; Song et al. 2022). Soils with higher CEC and larger SSA provide more adsorption sites for water molecules on particle surfaces and increase the opportunities for water molecules to interact with the surface, thereby accelerating the water vapour adsorption rate. Accordingly, the monolayer sorption rates (R_{a0} and R_{d0}) showed highly significant positive correlations with CEC and SSA_{H2O}. During adsorption, abundant vacant sites on the particle surface enable rapid attachment of water molecules through hydration forces, leading to the gradual formation of a monolayer. In contrast, during desorption, water molecules must overcome strong binding forces (e.g., hydration forces) to be released as a_w decreases (Figure 5a). Such differences in energy barriers account for the markedly higher R_{a0} compared to R_{d0}.

Due to the influence of hydration forces, water molecules adsorbed during monolayer adsorption exhibit an ordered structure. Once the monolayer adsorption is completed, as a_w increases, hydrogen bonds formed by water–water interactions cause additional water molecules from the environment to be adsorbed onto the outer layer of the monolayer. This process gradually thickens the water film and results in the formation of multiple layers. The ordered structure of the monolayer facilitates a certain degree of order in the multilayered water molecules as well (Asay and Kim 2005; Wong et al. 2022). Higher monolayer adsorption increases the opportunities for water molecule interactions, resulting in a higher rate of water vapour adsorption (Figure 5b). Consequently, the multilayer sorption rates (R_{am} and R_{dm}) also exhibit a highly significant positive correlation with CEC and SSA_{H2O}. During multilayer adsorption, adsorption and desorption occur at surface sites on soil particles that are already fully occupied by water molecules. These processes mainly involve the formation and disruption of hydrogen bonds, which have relatively low bond energies. Due to the minimal difference in the number of adsorption sites and surface forces between adsorption and desorption processes, the difference between R_{am} and R_{dm} was small.

During the capillary condensation, the water molecule layer on the surface of soil particles thickens, and condensed water begins to occupy nanometre-scale pores (2–200 nm in diameter) within the soil (Figure 5c). Inside these pores, water molecules increasingly exhibit the structure characteristic of liquid water (Boudot et al. 2016; Chen et al. 2021; Wong et al. 2022). During adsorption, the vapour pressure of water outside the pores exceeds that within the pores, promoting the diffusion and condensation of water molecules into the pores. As adsorption progresses, the vapour pressure inside the pores gradually increases, reducing the pressure difference between the interior and exterior of the pores (Figure 5c). This reduction in pressure difference slows the diffusion rate of water molecules into the pores and prolongs the time required to reach adsorption equilibrium (Scott and Dullien 1962). In the capillary condensation phase, the significant positive correlation between adsorption time and PV ($R^2=0.96$) provides further evidence for this mechanism (Figure 6). Akin and Likos (2020) also found that the adsorption time during the condensation process was longer than the desorption time. Due to the diffusion limitation, the R_a decreased with increasing a_w at high a_w range (> ~0.8). Song et al. (2022) reported that PV is a key factor influencing soil water vapour adsorption capacity during the condensation process. However, in this study, no significant correlation was observed between R_{ac} and PV (Figure 4). This discrepancy might be attributed to the low diffusion rate of water molecules within pores during adsorption. As a result, the factors influencing the adsorption rate at this stage were consistent with those at low a_w, showing a positive correlation with CEC and SSA_{H2O} (Figure 4). In contrast, the vapour pressure inside the pores is higher than that of the external environment during desorption, facilitating the diffusion of water molecules from the pores to the surroundings (Figure 5c). Consequently, larger PV values correspond to higher desorption rates during condensation. Generally, finer soil particles have a larger SSA_{N2}, which is often associated with a greater PV (Song et al. 2022). Therefore, in addition to its strong positive correlation with PV, the R_{dc} also showed a positive correlation with clay content and SSA_{N2}. Moreover, the influence of pores on water molecule diffusion during adsorption resulted in R_{ac} being lower than R_{dc}. Overall, R_{dc} was greater than R_{a0}, while R_{d0} was lower than R_{ac}, so the R_d had a larger variation range relative to R_a.

The differences in water vapour adsorption and desorption rates across the three processes primarily arise from variations in adsorption site availability, surface interaction forces, and adsorption kinetics. In the initial adsorption, soil particle surfaces provide abundant adsorption sites, allowing water molecules from the environment to be rapidly adsorbed onto the surface through hydration forces to form a monolayer (Lu and Khorshidi 2015). As a_w increases, these sites become progressively occupied, and additional water molecules are subsequently adsorbed through weaker hydrogen bonding, gradually forming multilayers of water molecules (Asay and Kim 2005). With further increases in a_w, water molecules begin to condense on particle surfaces and within soil pores (Chen et al. 2021; Wong et al. 2022). However, diffusion constraints within pores slow the adsorption rate (Scott and Dullien 1962). Consequently, the R_a follow the order $R_{a0} > R_{am} > R_{ac}$. In the early stage of desorption, liquid water present on particle surfaces and within pores easily diffuses into the environment as a_w decreases, resulting in a relatively high R_d. As a_w continues to decrease, desorption shifts to multilayer-adsorbed water, which requires breaking weak hydrogen bonds, and finally to monolayer-adsorbed water, which demands overcoming stronger hydration forces. Thus, the R_d follow the order $R_{dc} > R_{dm} > R_{d0}$.

Soil water vapour adsorption and desorption are key processes governing vapour transport in arid areas. Field monitoring results in such areas showed that the a_w of the atmosphere and soil pores varied from ~0.25 to 1 (Goss and Madliger 2007; Yang et al. 2017; Lopez-Canfin et al. 2022), indicating that sorption processes predominantly occur in the multilayer adsorption and capillary condensation stages. When the microenvironment changes from dry ($a_w = \sim 0.3$) to wet ($a_w > 0.8$), the soil will adsorb water molecules from the air, and the R_a is mainly related to soil surface properties (e.g., SSA and CEC). Larger SSA and higher CEC generally result in faster R_a. Conversely, when the microenvironment changes from wet to dry, adsorbed water molecules will desorb, and the R_d depends on both surface properties and nano-scale pores. From the measured data of a_w in arid areas, the R_d is generally faster than the R_a. This study investigated the changes of R_a and R_d with a_w and their influencing factors under isothermal conditions. In the field, however, both temperature and a_w fluctuate substantially. For example, the a_w of the atmosphere in arid areas during the day can reach as low as ~0.3, and the maximum temperature can reach 50°C. The a_w at night can reach ~0.95, and the minimum temperature can reach 0°C

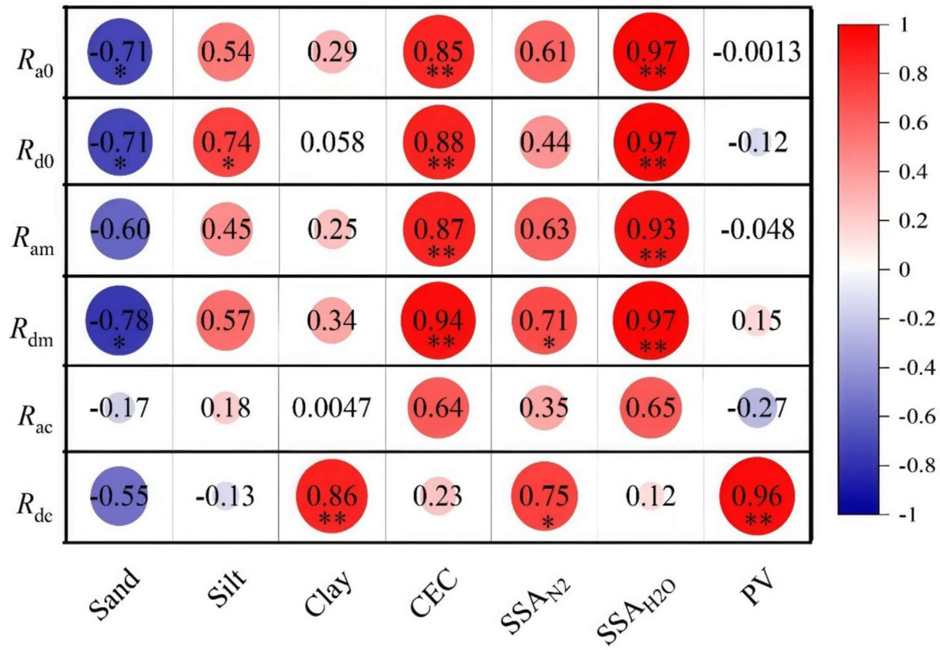

FIGURE 4 | Heat map of correlation between adsorption/desorption rates of eight mineral soils and physicochemical properties. The R_{a0}/R_{d0}, R_{am}/R_{dm}, and R_{ac}/R_{dc} are the adsorption/desorption rates during the monolayer adsorption ($0.05 < a_w < 0.2$), multilayer adsorption ($0.2 < a_w < 0.6$), and condensation processes ($0.6 < a_w < 0.93$), respectively. A single asterisk (*) indicates a significant correlation at $p < 0.05$, and a double asterisk (**) indicates a significant correlation at $p < 0.01$.

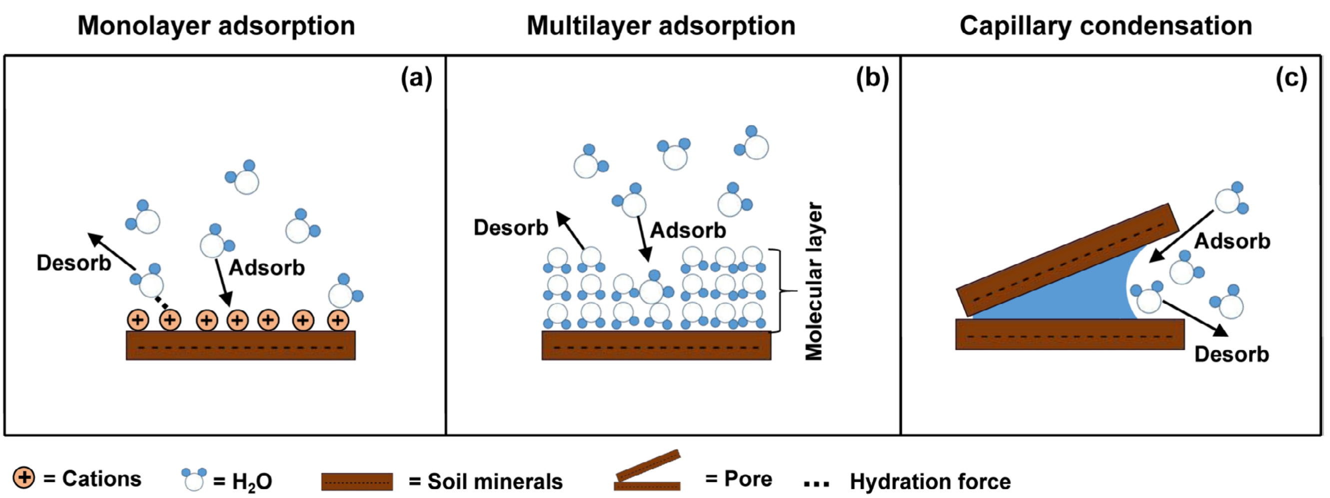

FIGURE 5 | Schematic diagrams of soil water vapour adsorption and desorption kinetics during the monolayer adsorption ($0.05 < a_w < 0.2$) (a), multilayer adsorption ($0.2 < a_w < 0.6$) (b), and capillary condensation processes ($0.6 < a_w < 0.93$) (c), respectively.

(Goss and Madliger 2007). The impact of such large temperature changes on the dynamics of soil water vapour sorption is still unclear. Additionally, the experimental findings derived from controlled laboratory experiments cannot be directly extrapolated to heterogeneous field environments due to oversimplified boundary conditions. Future research should focus on quantifying the effects of temperature fluctuations (e.g., diurnal thermal gradients, seasonal variations) on soil water vapour sorption kinetics. Furthermore, coupling controlled laboratory studies with field-based in situ experiments will be essential to unravel the mechanisms governing water vapour adsorption and transport processes under natural boundary conditions.

5 | Conclusions

The magnitude of soil water vapour adsorption rate depends on the adsorption process and direction, as well as soil physicochemical properties. Specifically, the adsorption rate (R_{a0}) was higher than the desorption rate (R_{d0}) for monolayer adsorption, and the adsorption and desorption rates (R_{am} and R_{dm}) showed no significant difference for multilayer adsorption, and the adsorption rate (R_{ac}) was lower than the desorption rate (R_{dc}) for the condensation process. The R_{a0}, R_{d0}, R_{am}, R_{dm}, and R_{ac} were closely related to cation exchange capacity and total specific surface area, and the R_{dc} was closely related to clay content,

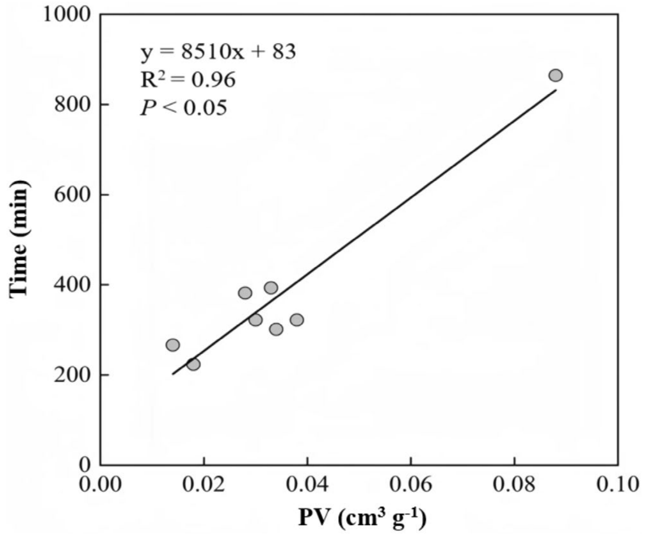

FIGURE 6 | Correlation analysis between adsorption duration and pore volume (PV) during condensation processes ($0.6 < a_w < 0.93$) for investigated eight soils.

external specific surface area, and pore volume. Soil water vapour adsorption and desorption are important processes in the exchange of water between soil and atmosphere in arid regions. The findings of this study are very helpful for an in-depth understanding of soil water vapour movement processes in these environments. However, these findings were derived from controlled laboratory conditions, which may oversimplify the complexity of natural environments and limit direct extrapolation to heterogeneous field settings. Future studies should explore the impact of temperature fluctuations, including diurnal and seasonal variations, on soil water vapour sorption dynamics. Integrating laboratory experiments with field-based in situ investigations will be essential to comprehensively understand the mechanisms governing water vapour adsorption and transport under natural conditions.

Author Contributions

Zizheng Deng: data curation, formal analysis, writing – original draft, methodology. **Chong Chen:** conceptualization, funding acquisition, writing – review and editing. **Xue Song:** data curation, formal analysis. **Jianying Shang:** resources, supervision. **Hu Zhou:** resources, supervision.

Conflicts of Interest

The authors declare no conflicts of interest.

Data Availability Statement

The data that support the findings of this study are available from the corresponding author upon reasonable request.

References

Agam, N., and P. R. Berliner. 2006. "Dew Formation and Water Vapor Adsorption in Semi-Arid Environments—A Review." *Journal of Arid Environments* 65, no. 4: 572–590. https://doi.org/10.1016/j.jaridenv.2005.09.004.

Akin, I. D., and W. J. Likos. 2014. "Specific Surface Area of Clay Using Water Vapor and EGME Sorption Methods." *Geotechnical Testing Journal* 37, no. 6: 1016–1027. https://doi.org/10.1520/GTJ20140064.

Akin, I. D., and W. J. Likos. 2020. "Relationship Between Water Vapor Sorption Kinetics and Clay Surface Properties." *Journal of Geotechnical and Geoenvironmental Engineering* 146, no. 9: 0602001. https://doi.org/10.1061/(ASCE)GT.1943-5606.0002337.

Araya, S. N., M. Meding, and A. A. Berhe. 2016. "Thermal Alteration of Soil Physico-Chemical Properties: A Systematic Study to Infer Response of Sierra Nevada Climosequence Soils to Forest Fires." *Soil* 2, no. 3: 351–366. https://doi.org/10.5194/soil-2-351-2016.

Asay, D. B., and S. H. Kim. 2005. "Evolution of the Adsorbed Water Layer Structure on Silicon Oxide at Room Temperature." *Journal of Physical Chemistry B* 109, no. 35: 16760–16763. https://doi.org/10.1021/jp053042o.

Boudot, M., H. Elettro, and D. Grosso. 2016. "Converting Water Adsorption and Capillary Condensation Into Usable Forces With Simple Porous Inorganic Thin Films." *ACS Nano* 10, no. 11: 10031–10040. https://doi.org/10.1021/acsnano.6b04648.

Brunauer, S., P. H. Emmett, and E. Teller. 1938. "Adsorption of Gases in Multimolecular Layers." *Journal of the American Chemical Society* 60: 309–319. https://doi.org/10.1021/ja01269a023.

Cases, J. M. 1997. "Mechanism of Adsorption and Desorption of Water Vapor by Homoionic Montmorillonite: 3. The Mg2+, Ca2+, Sr2+ and Ba2+ Exchanged Forms." *Clay and Clay Minerals* 45, no. 1: 8–22. https://doi.org/10.1346/CCMN.1997.0450102.

Chen, C., E. Arthur, H. Zhou, et al. 2021. "A New Model for Soil Water Vapor Sorption Isotherms Considering Adsorption and Condensation." *Soil Science Society of America Journal* 85, no. 2: 195–206. https://doi.org/10.1002/saj2.20181.

Chen, C., Y. Jiang, B. Sun, H. Zhou, and P. D. Hallett. 2022. "Organic Manure and Lime Change Water Vapour Sorption of a Red Soil by Altering Water Repellency and Specific Surface Area." *European Journal of Soil Science* 73, no. 2: e13223. https://doi.org/10.1111/ejss.13223.

Chen, J., C. Shang, M. J. Eick, and R. D. Stewart. 2018. "Water Repellency Decreases Vapor Sorption of Clay Minerals." *Water Resources Research* 54, no. 9: 6114–6125. https://doi.org/10.1029/2018WR023352.

Cheng, W., K. Hanna, and J. F. Boily. 2019. "Water Vapor Binding on Organic Matter-Coated Minerals." *Environmental Science & Technology* 53, no. 3: 1252–1257. https://doi.org/10.1021/acs.est.8b05134.

Chiang, F., O. Mazdiyasni, and A. AghaKouchak. 2021. "Evidence of Anthropogenic Impacts on Global Drought Frequency, Duration, and Intensity." *Nature Communications* 12, no. 1: 2754. https://doi.org/10.1038/s41467-021-22314-w.

Gee, G. W., and D. Or. 2002. "Particle-Size Analysis." In *Methods of Soil Analysis. Part 4. SSSA Book Series No. 5*, edited by J. H. Dane and G. C. Topp, 255–293. SSSA.

Goss, K. U., and M. Madliger. 2007. "Estimation of Water Transport Based on In Situ Measurements of Relative Humidity and Temperature in a Dry Tanzanian Soil." *Water Resources Research* 43, no. 5: W05433. https://doi.org/10.1029/2006WR005197.

Grismer, M. E. 1987. "Vapor Adsorption Kinetics and Vapor Diffusivity." *Soil Science* 144, no. 1: 1–5. https://doi.org/10.1097/00010694-198707000-00001.

Hatch, C. D., J. S. Wiese, C. C. Crane, K. J. Harris, H. G. Kloss, and J. Baltrusaitis. 2012. "Water Adsorption on Clay Minerals as a Function of Relative Humidity: Application of BET and Freundlich Adsorption Models." *Langmuir* 28, no. 3: 1790–1803. https://doi.org/10.1021/la2042873.

Khorshidi, M., and N. Lu. 2017. "Intrinsic Relation Between Soil Water Retention and Cation Exchange Capacity." *Journal of Geotechnical and Geoenvironmental Engineering* 143, no. 4: 04016119. https://doi.org/10.1061/(ASCE)GT.1943-5606.0001633.

Kidron, G. J., and A. Starinsky. 2019. "Measurements and Ecological Implications of Non-rainfall Water in Desert Ecosystems—A Review." *Ecohydrology* 12, no. 6: e2121. https://doi.org/10.1002/eco.2121.

Kool, D., E. Agra, A. Drabkin, et al. 2021. "The Overlooked Non-Rainfall Water Input Sibling of Fog and Dew: Daily Water Vapor Adsorption on a! Nara Hummock in the Namib Sand Sea." *Journal of Hydrology* 598: 126420. https://doi.org/10.1016/j.jhydrol.2021.126420.

Kosmas, C., N. G. Danalatos, J. Poesen, and B. Van Wesemael. 1998. "The Effect of Water Vapour Adsorption on Soil Moisture Content Under Mediterranean Climatic Conditions." *Agricultural Water Management* 36, no. 2: 157–168. https://doi.org/10.1016/S0378-3774(97)00050-4.

Li, J., X. Li, K. Wu, et al. 2016. "Water Sorption and Distribution Characteristics in Clay and Shale: Effect of Surface Force." *Energy & Fuels* 30, no. 11: 8863–8874. https://doi.org/10.1021/acs.energyfuels.6b00927.

Lopez-Canfin, C., R. Lazaro, and E. P. Sanchez-Canete. 2022. "Water Vapor Adsorption by Dry Soils: A Potential Link Between the Water and Carbon Cycles." *Science of the Total Environment* 824: 153746. https://doi.org/10.1016/j.scitotenv.2022.153746.

Low, P. F. 1961. "Physical Chemistry of Clay-Water Interaction." *Advances in Agronomy* 13: 269–327.

Lu, N., and M. Khorshidi. 2015. "Mechanisms for Soil-Water Retention and Hysteresis at High Suction Range." *Journal of Geotechnical and Geoenvironmental Engineering* 141, no. 8: 04015032. https://doi.org/10.1061/(ASCE)GT.1943-5606.0001325.

Mishra, A. K., and V. P. Singh. 2010. "A Review of Drought Concepts." *Journal of Hydrology* 391, no. 1–2: 202–216. https://doi.org/10.1016/j.jhydrol.2010.07.012.

Sang, G., S. Liu, and D. Elsworth. 2019. "Water Vapor Sorption Properties of Illinois Shales Under Dynamic Water Vapor Conditions: Experimentation and Modeling." *Water Resources Research* 55, no. 8: 7212–7228. https://doi.org/10.1029/2019WR024992.

Scott, D. S., and F. A. L. Dullien. 1962. "Diffusion of Ideal Gases in Capillaries and Porous Solids." *AICHE Journal* 8, no. 1: 113–117. https://doi.org/10.1002/aic.690080126.

Song, X., C. Chen, E. Arthur, et al. 2022. "Cation Exchange Capacity and Soil Pore System Play Key Roles in Water Vapour Sorption." *Geoderma* 424: 116017. https://doi.org/10.1016/j.geoderma.2022.116017.

Song, X., C. Chen, H. Zhou, J. Shang, and T. Ren. 2023. "Effect of High-Temperature Treatment on Water Vapour Sorption of Montmorillonite." *Geoderma* 436: 116563. https://doi.org/10.1016/j.geoderma.2023.116563.

Spinoni, J., G. Naumann, H. Carrao, P. Barbosa, and J. Vogt. 2014. "World Drought Frequency, Duration, and Severity for 1951–2010." *International Journal of Climatology* 34, no. 8: 2792–2804. https://doi.org/10.1002/joc.3875.

Sumner, M. E., and W. P. Miller. 1996. "Cation Exchange Capacity and Exchange Coefficients." In *Methods of Soil Analysis. Part 3 – Chemical Methods*, edited by D. L. Sparks, A. L. Page, P. A. Helmke, and R. H. Loeppert, 1201–1229. American Society of Agronomy, Soil Science Society of America.

Sun, F., B. Xiao, G. J. Kidron, and J. Heitman. 2024. "Biocrusts Critical Regulation of Soil Water Vapor Transport (Diffusion, Sorption, and Late-Stage Evaporation) in Drylands." *Water Resources Research* 60, no. 7: e2023WR036520. https://doi.org/10.1029/2023WR036520.

Tuller, M., D. Or, and L. M. Dudley. 1999. "Adsorption and Capillary Condensation in Porous Media: Liquid Retention and Interfacial Configurations in Angular Pores." *Water Resources Research* 35, no. 7: 1949–1964. https://doi.org/10.1029/1999WR900098.

van den Berg, C., and S. Bruin. 1981. "Water Activity and Its Estimation in Food Systems." In *Water Activity: Influences on Food Quality*, edited by L. B. Rockland and G. F. Stewart, 147–177. Academic.

Verhoef, A., A. Díaz-Espejo, J. R. Knight, L. Villagarcía, and J. E. Fernandez. 2006. "Adsorption of Water Vapor by Bare Soil in an Olive Grove in Southern Spain." *Journal of Hydrometeorology* 7, no. 5: 1011–1027. https://doi.org/10.1175/JHM556.1.

Wang, Y., S. Lu, T. Ren, and B. Li. 2011. "Bound Water Content of Air-Dry Soils Measured by Thermal Analysis." *Soil Science Society of America Journal* 75, no. 2: 481–487. https://doi.org/10.2136/sssaj2010.0065.

Wong, E. V. S., P. R. Ward, M. Leopold, D. V. Murphy, and L. Barton. 2022. "Condensation of Capillary Water and Decreased Surface Energy Cause Increased Soil Water Repellency in Sandy Soil." *European Journal of Soil Science* 73, no. 6: e13325. https://doi.org/10.1111/ejss.13325.

Xiong, S., M. Chen, H. Yu, et al. 2023. "Experimental Investigation of Thermodynamic and Kinetic Behaviors From Water Vapor Adsorption on Four Typical Clay Minerals." *Gas Science and Engineering* 111: 204933. https://doi.org/10.1016/j.jgsce.2023.204933.

Yang, P., G. Ren, and W. Hou. 2017. "Temporal–Spatial Patterns of Relative Humidity and the Urban Dryness Island Effect in Beijing City." *Journal of Applied Meteorology and Climatology* 56, no. 8: 2221–2237. https://doi.org/10.1175/JAMC-D-16-0338.1.

Yeşilbaş, M., and J. F. Boily. 2016. "Particle Size Controls on Water Adsorption and Condensation Regimes at Mineral Surfaces." *Scientific Reports* 6, no. 1: 32136. https://doi.org/10.1038/srep32136.

Supporting Information

Additional supporting information can be found online in the Supporting Information section. **TABLE S1:** Relative content of the main clay minerals for investigated eight soils.